Caterina Vigliar: catvi@dtu.dk
Mujtaba Zahidy: muzah@dtu.dk

HSOC Group, DTU ELECTRO
Teaching assistants: Damien Roux, Inaki Beraza.

Bell state generation on a photonic chip

System setup and characterization

Quantum Lab at the Quantum Communication Systems Group at DTU ELECTRO

Experimental lab session: 8 hours

Data analysis and poster creation: 4 hours

General lab session objective

The primary goal of this laboratory experience is to introduce students to the principles and techniques involved in generating photonic entangled states on integrated devices and in measuring them with high fidelity. The laboratory session will be dedicated to evaluating key performance metrics for validating the operation of photonic quantum integrated circuits, including integrated interferometer calibration, photon-pair generation efficiency, and quantum state fidelity.

Learning objectives

By the end of the session, the student will be able to:

1. Explain the basic principles of how superposition and entanglement can be created with on-chip spontaneous photon-pair sources and linear-optical elements in post-selection.
2. Explain the details of implementing unitary operations and projective measurements on simple quantum states with on-chip linear optical elements (focus on Pauli operations).
3. Operate simple integrated optical setups (common lab practices and basic optical characterization).
4. Extract performance parameters from observed classical and quantum optical data (Mach-Zehnder fringes, pulsed laser spectrum, spontaneous four-wave-mixing histograms, Pauli projective measurements).
5. Characterize and operate a realistic Silicon/Silicon Nitride implementation of a two-qubit Bell state generator.
6. Extract Pauli measurements probability outcomes from experimental data using one of the above setups and reconstruct a Bell state's density matrix.
7. Calculate quantum state fidelity to evaluate the quality of the Bell state generator.
8. Discuss the obtained results in groups and clearly illustrate them through a poster presentation, discussing possible sources of error and ways to overcome them.
9. Discuss the challenges of real implementations of post-selected photonic Bell-state generation (scalability to larger states in relation to chip performance).

Lab experience structure

The lab session will be structured as follows:

- **Lab tour and safety briefing**: we will give an overview of the activities in the Quantum Communication Systems Lab and discuss lab safety and laser safety and the importance of

handling equipment properly. Explanation of what happens if one ignores the safety regulations.

- **Theoretical briefing**: short theoretical lecture on the basic building blocks of integrated photonics and how to realize two-qubit Bell states with on-chip spontaneous photon-pair sources and linear-optical elements in post-selection.
- **Silicon and Silicon Nitride setups**: The students will be divided in two subgroups of 5-6 students each: one working on a Silicon device in the Quantum Lab, one working on a Silicon Nitride device in the Wireless Lab.
- **Building blocks characterization**: Setup and measurement of Mach-Zehnder interferometer optical fringes. Discussion and exercise about the techniques adopted for their calibration.
- **Pulsed laser working principles**: introduction on how to generate high-power short duty-cycle laser pulses. Discussion and exercise about how to estimate a pulsed laser's peak power.
- **Spontaneous Photon-pair source characterization**: visualization of coincidence histograms from a Silicon spiral source under different pulsed pump laser powers. Discussion about the meaning of coincidence histogram peaks and the estimation of the photon pair generation parameter.
- **Performance of a Bell state full tomography experiment**: data acquisition of projective Pauli measurements through superconducting single photon detection.
- **Data analysis:** reconstruction of a two-qubit density matrix and calculation of the reconstructed state's fidelity against the expected theoretical state
- **Poster production**

The session will be conducted in two groups of approximately 6-7 students each: one working on the Silicon setup (with Caterina), one on the Silicon Nitride setup (with Mujtaba). Sub-teams of 3-4 students will be formed throughout the session to ensure that everyone has hands-on experience with each part of the setup.

Day 1 (Thursday @ DTU Electro, Building 340, Lab 1.16)	
Silicon Group – Quantum Lab	Silicon Nitride Group – Wireless Lab
9:00 - 9.20 Quantum Communication Systems Lab Tour	
9:20 – 9:50 Theory briefing (Caterina – Wireless Lab)	
10:00 – 10:40 Mach-Zehnder Characterization	**10:00 – 10:40** Mach-Zehnder Characterization
10:40 – 12:00 Mode-locked laser exercise (Mujtaba – Wireless Lab)	
Lunch break	
13:30 – 14:20 Spontaneous four-wave-mixing photon sources (Caterina – Quantum Lab)	
14:30 – 16:30 Quantum State Tomography	**14:30 – 16:30** Quantum State Tomography

Day 2 (Tuesday @ anywhere arranged among subgroups)
9:00 – 12:00 data analysis and poster production (groups of 4 students max)

Caterina Vigliar: catvi@dtu.dk
Mujtaba Zahidy: muzah@dtu.dk

HSOC Group, DTU ELECTRO
Teaching assistants: Damien Roux, Inaki Beraza.

Introduction

The greatest challenge of all the efforts aimed at the development of quantum technologies is the engineering of a set of well-characterized two-level quantum systems — quantum bits or qubits. To ultimately compute arbitrary quantum information processing tasks accurately and efficiently, qubits have to be easily initialisable, processable by a universal gate set, and measurable with high fidelity on a scalable physical platform, i.e. a physical system whose resources grow at most polynomially with the number of generated and manipulated qubits [1]. Moreover, such two-level systems must have long decoherence times, much longer than the gate operation time, and must have low interactions with the environment to preserve their state during long computations. If this condition is not satisfied, the quantum state of a qubit would soon decohere into a classical mixed state, leading quantum algorithms to failure.

Many of the requirements needed to perform quantum information processing can be found in existing proposals, with qubits being defined by single atoms [2-3], single electrons [4], or by more complicated systems, like very cold superconducting electrical circuits in which electrons move [5]. One of the most appealing platforms for satisfying the conditions necessary for constructing a quantum computer is photonics. In this lab experience, we will focus on photonic qubits, i.e. quantum bits carried by single photons — the fundamental particles of light. Photons are an attractive physical system for representing qubits for many different reasons. They can encode qubits in different ways, regarding which of their dichotomic characteristics is considered: polarization, time-bin, frequency, orbital angular momentum, spatial mode or path. They not only provide a scalable system of robust, well-characterized quantum bits, with robust physical representations that retain their quantum properties, but are also systems in which qubits can evolve as desired by a universal set of unitary transformations, including single-qubit gates and two-qubit controlled gates able to build entanglement by using interference and measurement. Moreover, quantum states can be generated with high fidelity and with long coherence times, maintaining the correct encoding of the information even when guided along long distances in optical fibers. Finally, they have a reliable read-out technique, with recently developed superconducting nano-wire single-photon detectors displaying measurement efficiencies up to 98% [6].

The following section is intended to provide a general background on photonic quantum information processing, focusing on how qubits can be encoded, manipulated and measured using photonic states and linear optical components in integrated devices. Please not the following that this introductory section has been largely simplified. References and further reading material are given for interested readers at the end of this document.

Caterina Vigliar: catvi@dtu.dk
Mujtaba Zahidy: muzah@dtu.dk
HSOC Group, DTU ELECTRO
Teaching assistants: Damien Roux, Inaki Beraza.

Quantum information processing with linear optics

Single photons for qubit encodings

In the second quantisation formalism, light is described as an ensemble of quantum harmonic oscillators with Hamiltonian [7]

$$\hat{H} = \sum_k \hat{H}_k, \quad \text{with} \quad \hat{H}_k = \hbar\omega_k\left(\hat{a}_k^\dagger \hat{a}_k + \frac{1}{2}\right),$$

where each Hamiltonian $\hat{H}_k$ refers to a single harmonic oscillator with angular frequency ω_k associated with the k-th mode of the electromagnetic field. These modes can be, for example, spatial modes, spectral modes, polarisations, and so on. In this course, we will consider *spatial modes*, for instance, *waveguides in a photonic chip*. The operators $\hat{a}_k^\dagger$ and $\hat{a}_k$ are bosonic creation and annihilation operators for excitations in the mode k, and obey the bosonic commutation rules. Photons represent the single bosonic quantum excitations of the electromagnetic field. The photonic states are indicated via Fock vectors $|n\rangle_k$, where n represents the number of photons in mode k, and satisfy [7]

$$\hat{a}_k^\dagger |n\rangle_k = \sqrt{n+1}\,|n+1\rangle_k, \quad \hat{a}_k |n\rangle_k = \sqrt{n}\,|n-1\rangle_k \quad \text{and} \quad \hat{N}_k = \hat{a}_k^\dagger \hat{a}_k,$$

where $\hat{N}_k$ is the number operator on mode k. Photons occupying the same optical mode are said to be *indistinguishable*, and are *distinguishable* otherwise. The state $|0\rangle_k$, in which no photons are present in the k-th mode, is the vacuum state associated to mode k. Any Fock state can be written as

$$|n\rangle_k = \frac{1}{\sqrt{n!}}\left(\hat{a}_k^\dagger\right)^n |0\rangle_k .$$

In a configuration where a total of $n = \sum_{k=1}^{m} n_k$ photons are in m different modes, where the k-th mode contains n_k photons, the total Fock state of the system is given by the tensor product of the Fock states for each mode:

$$|\mathbf{n}\rangle = |n_1 n_2 \ldots n_m\rangle = |n_1\rangle \otimes |n_2\rangle \otimes \ldots \otimes |n_m\rangle .$$

This class of states forms an orthogonal basis of the Hilbert space $\mathcal{H}_m^n$ of n indistinguishable photons in m modes. An arbitrary state of n photons in m modes can thus be written as the superposition

$$|\psi\rangle = \sum_n \beta_n |\mathbf{n}\rangle ,$$

where n ranges over all possible configurations $(n_1, n_2, \ldots, n_m)$ with a fixed total number of photons and $\sum_k |\beta_k|^2 = 1$. Fock states can be used to define qubits in many ways. In this course, we will focus on dual-rail qubits, whereby two modes are used to encode a qubit: the presence of a photon in the first mode encodes the $|0\rangle$ state and the presence of a photon in the other encodes the $|1\rangle$ state (see Fig. 1.A). When we look at the path taken by the photon, we say that the qubit is *encoded in the path degree of freedom*. Multiple-level systems (qudits) can be easily encoded by increasing the number of paths a photon can take (see Fig. 1.B).

Caterina Vigliar: catvi@dtu.dk
Mujtaba Zahidy: muzah@dtu.dk
HSOC Group, DTU ELECTRO
Teaching assistants: Damien Roux, Inaki Beraza.

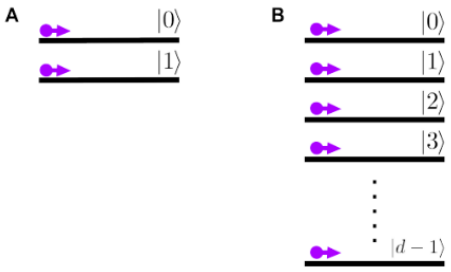

Figure 1: Photonic qubit and qudit path encoding. ***A.*** *The presence of a photon over two spatial modes encodes a qubit.* ***B.*** *The presence of a photon over d spatial modes encodes a qudit.*

Linear optical building blocks in integrated photonics

To make photonic qubits useful for quantum computing applications, it is crucial to be able to define a set of universal gates in the encoding described above, i.e. a set of gates that are sufficient to approximate any unitary operation to an arbitrary accuracy via a quantum circuit. This goes through the implementation of arbitrary single-qubit gates and two-qubit entangling gates such as the controlled-not gate (CX) or the controlled-phase gate (CZ). The control and manipulation of such qubits is accomplished by using combinations of beam-splitters and phase shifters. In the following section, we will give a brief review of linear optics and show in more detail how optical operations can be implemented in integrated optical environments.

Arbitrary operations on dual-rail qubits can be described by transformations of the optical modes (Bogoliubov transformations that do not mix the creation and annihilation operators, usually described as passive):

$$\hat{a}_1^\dagger \rightarrow \hat{a}_1'^\dagger = \alpha_{11}\hat{a}_1^\dagger + \alpha_{12}\hat{a}_2^\dagger$$
$$\hat{a}_2^\dagger \rightarrow \hat{a}_2'^\dagger = \alpha_{21}\hat{a}_1^\dagger + \alpha_{22}\hat{a}_2^\dagger.$$

Here, the transformation

$$\hat{U} = \begin{pmatrix} \alpha_{11} & \alpha_{12} \\ \alpha_{21} & \alpha_{22} \end{pmatrix}$$

is a unitary matrix. These mode transformations can be decomposed into beam-splitter transformations (with reflectivity r) and phase-shifter transformations (with phase ϕ):

$$\hat{U}_{BS}(r) = \begin{pmatrix} \sqrt{r} & i\sqrt{1-r} \\ i\sqrt{1-r} & \sqrt{r} \end{pmatrix}, \quad \hat{U}_{PS}(\phi) = \begin{pmatrix} 1 & 0 \\ 0 & e^{i\phi} \end{pmatrix}.$$

A phase-shifter with phase ϕ, embedded between two balanced beam-splitters, forms a *Mach-Zehnder interferometer (MZI)*, which is equivalent, up to a global phase, to a beamsplitter with variable reflectivity $r = sin^2(\varphi/2)$. If, for simplicity, we label with $\hat{U}_{BS}$ the unitary matrix corresponding to a balanced (50% reflectivity) beam-splitter, we can write the overall MZI unitary as follows:

Caterina Vigliar: catvi@dtu.dk
Mujtaba Zahidy: muzah@dtu.dk
HSOC Group, DTU ELECTRO
Teaching assistants: Damien Roux, Inaki Beraza.

$$\hat{U}_{MZI}(\varphi) = \hat{U}_{BS}\hat{U}_{PS}(\varphi)\hat{U}_{BS} = ie^{-i\varphi/2}\begin{pmatrix}\sin(\varphi/2) & \cos(\varphi/2)\\ \cos(\varphi/2) & -\sin(\varphi/2)\end{pmatrix},$$

where φ indicates the phase shift on the beam-splitter's reflected arm. If we add another phase-shifter (ϕ_1) to the MZI we can achieve a general mode transformation

$$\hat{U} = \hat{U}_{BS}\hat{U}_{PS}(\varphi)\hat{U}_{BS}\hat{U}_{PS}(\phi_1) = ie^{-i\varphi/2}\begin{pmatrix}e^{i\phi_1}\sin(\varphi/2) & e^{i\phi_1}\cos(\varphi/2)\\ \cos(\varphi/2) & -\sin(\varphi/2)\end{pmatrix}.$$

It is important to note that not all qubit transformations are rotations in the Bloch sphere, but some operations, like the Hadamard, are reflections with respect to a particular axis. To realise these transformations, an extra phase shift is added to the rotation (ϕ_2), as shown in Fig. 2. Any SU(2) matrix can therefore be decomposed in terms of Pauli rotations along the Z, Y and again Z axes:

$$\hat{U}(2) = \hat{R}_Z(\gamma)\hat{R}_Y(\beta)\hat{R}_Z(\alpha) = \hat{U}_{PS}(\phi_2)\hat{U}_{MZI}(\varphi)\hat{U}_{PS}(\phi_1),$$

with the second equality being valid up to global phases. Moreover, this setup allows us to map a given single-qubit basis to any other basis, not just any given state to any other state.

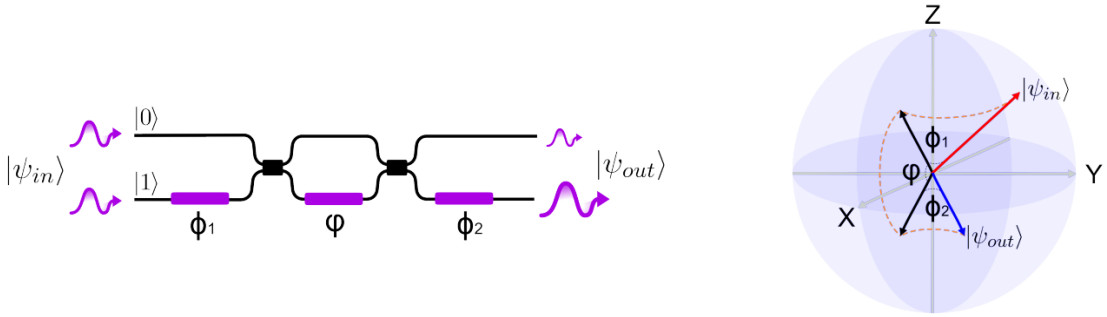

Figure 2: *Path-encoded arbitrary single-qubit gates with linear optics. A unitary transformation on a single qubit can be decomposed into three rotations along the Z, Y and again Z axes. On the left, its decomposition into beam-splitters and phase-shifters is shown.*

For the purpose of this course, we will consider only single-photon operations over two spatial modes. For more information on how to perform operations over multiple modes, refer to [8, 9]. For a detailed description on how to implement two-photon entangling operations exploiting measurement-induced non-linearities, refer to [10, 11]. For a general overview on how to combine all this to build a blueprint of a linear-optical quantum computer, refer to [12].

Caterina Vigliar: catvi@dtu.dk
Mujtaba Zahidy: muzah@dtu.dk

HSOC Group, DTU ELECTRO
Teaching assistants: Damien Roux, Inaki Beraza.

Integrated optical components in Silicon and Silicon Nitride chips

Silicon or Silicon Nitride chips can be successfully used to realize all the key components necessary for realising large-scale quantum photonic circuits, as shown in Fig. 3. We will narrow this description to the elements that will constitute the building blocks for the experiment performed in this course, overlooking on other, although relevant, integrated components. For a more complete list refer to [13, 14].

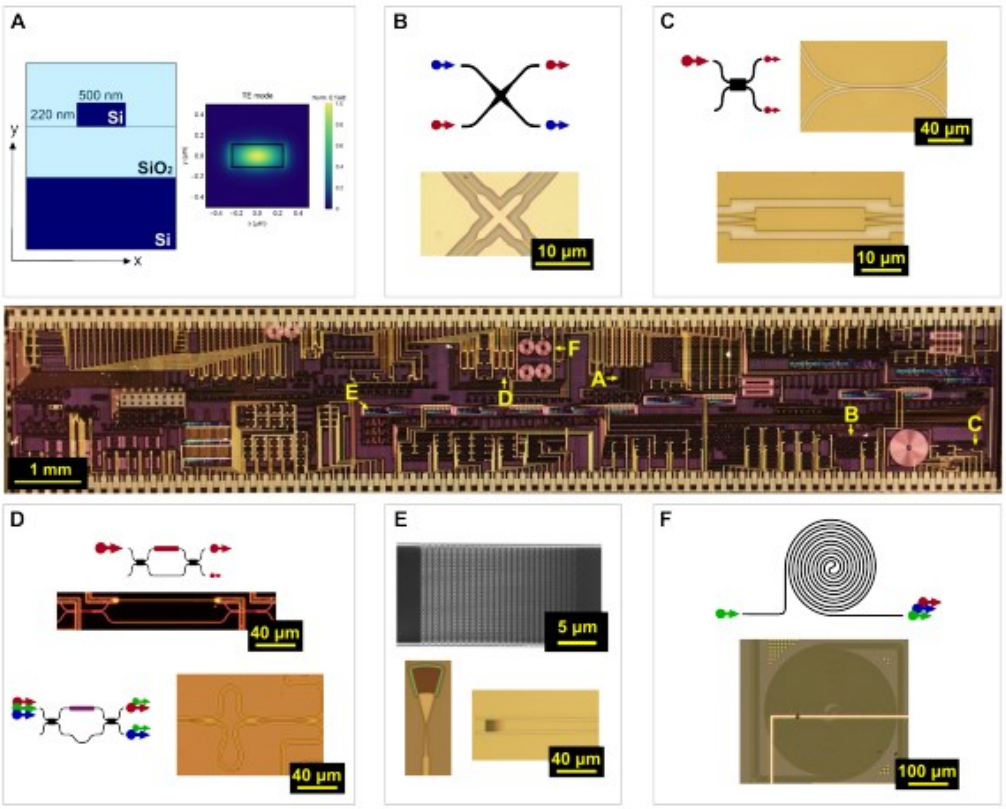

Figure 3: Integrated components in silicon. An example of a multi project wafer: in an area of dimension 16 × 2.8 mm several different experiments are present. The chip is illuminated with LED light to visualise circuits and integrated elements. A. Silicon waveguides, dimensions and single mode confinement. B. Crossers: schematics and SEM image. C. Directional couplers and MMIs: schematics and SEM image. D. Mach-Zehnder symmetric and asymmetric interferometers: schematics and microscope images. E. Grating couplers: standard and focussing structures. F. Spiral photon-pair sources.

Grating couplers and edge couplers: on-chip coupling

Grating couplers are periodic structures used to guide light in and out of integrated circuits, diffracting light from free space propagation (out of the chip plane) to waveguide propagation (in the chip plane). Given the huge mismatch between the waveguide mode dimensions (order of a hundred nanometers) and optical fibers mode dimensions (order of a few hundred micrometres), obtaining efficient fiber to

chip coupling, and vice versa, is a hard task. Currently, the highest grating efficiency coupling has been demonstrated with an insertion loss around 0.2 dB. Other techniques can be used exploring edge coupling which can lead to even lower coupling losses when using inverse taper designs to compensate for the mode mismatch. An optical microscope image of a grating coupler as seen from the top is shown in Fig.3E. Grating couplers and edge couplerscan be designed for any polarization, wavelength, spatial mode and coupling angle; they can also include gradual tapers to adiabatically focus in the integrated waveguides with low loss.

Multimode interferometers or MMIs

Multimode interferometers (MMIs) are integrated beam-splitters designed to be very resilient against fabrication variations. They are composed of two input single-mode waveguides brought together into a larger multi-mode region, where multiple higher-order modes are supported. As they propagate with different group velocities inside the multi-mode region, they accumulate different phases, giving rise to interference patterns with beatings. By appropriately tailoring the length of the multimode section, the output light can be collected exactly at the point where the image created by each input is equally split between the two outputs (see Fig. 3C). In this case, the transformation operated by the MMI is that of a balanced beam-splitter with transfer matrix:

$$U_{\mathrm{MMI}} = \frac{1}{\sqrt{2}} \begin{pmatrix} 1 & i \\ i & 1 \end{pmatrix}.$$

Crossers

In building circuits, light needs to be routed to the right places. Being the space limited to two dimensions, there will necessarily be the need of crossing light-paths. Crosser elements help to do this, allowing for waveguides swapping (see Fig. 3B). In this course crossers designed using multimode structures similar to the ones used for MMIs will be used, in which two multimode waveguides are crossed in the exact point where the first image of the input is created. In that point the two modes associated to the two inputs are orthogonal, thus avoiding crosstalk. Insertion loss in this structures can be very low, holding typical values of −0.1 dB per crosser.

Thermal phase shifters

The thermo-optic effect in silicon can be used for building phase shifters for path-encoded qubits. Changing the temperature of a waveguide's region can induce a localised change in the refractive index, which in turn induces a phase shift

$$\Delta\phi = \frac{2\pi L}{\lambda}\Delta n = \frac{2\pi L}{\lambda}\frac{dn_{\mathrm{eff}}}{dT}\Delta T.$$

To precisely control the phase in a waveguide, a resistive metal film is placed on top of it: the amount of power thermally dissipated in the metal film, and hence the temperature of the waveguide beneath, can be tuned by electrically controlling the voltage applied to it. Phases on the chip can thus be directly related to the voltages applied to each resistive element. Typical silicon waveguides, require a change in temperature as high as 100 K to obtain a full 2π phase shift, corresponding to a dissipated power of approximately 50 mW. This is why complex devices comprising several tens of phase shifters, as the ones we will use in this course, require techniques to carefully dissipate the heat

generated by the thermal phase shifters. Combined with two integrated beam-splitters, phase shifters can be used to build up Mach-Zehnder interferometers.

Photon-pair sources in integrated photonics

Over the last decade, a huge effort has been carried out to integrate photon sources themselves in silicon and silicon nitride chips, allowing a significant step forward against loss of signal [15, 16]. Usually, these exploit the non-linear properties of silicon or silicon nitride themselves, taking the form of long spiral waveguides or ring resonators in which spontaneous processes enable the generation of single photon pairs. However, with the present technology photon sources are still based on spontaneous processes, thus in most part highly inefficient (typical generatio efficiencies between 1-3%). Other approaches envisage the hybrid integration of solid-state-based photon sources within miniaturised photonic elements and circuits. For example, quantum dots could embody near-ideal single photon sources, with efficiencies higher than 90% and good indistinguishability [17], representing a very appealing route for future photonic implementations. Here, we will review on the most common photon-pair sources currently used in silicon and silicon nitride, based on *spontaneous four-wave mixing (SFWM)*. Despite being probabilistic, we can successfully fabricate them in arrays and control them simultaneously for the generation of tens of entangled photons.

Spontaneous Four-Wave Mixing and Third-Order Nonlinear Interactions

When light interacts with matter, the material's electrons respond to the electric field of the light, creating an induced polarization. In ordinary or *linear* optics, this polarization is directly proportional to the light's electric field. However, when the light intensity becomes very high—such as in the case of laser light—the response of the medium becomes *nonlinear*. This means the polarization includes higher-order terms in the electric field. Mathematically, it can be expressed as:

$$P = \varepsilon_0 \left(\chi^{(1)} E + \chi^{(2)} E^2 + \chi^{(3)} E^3 + \dots \right)$$

Here, $\chi^{(3)}$ represents the *third-order nonlinear susceptibility*, which gives rise to a range of nonlinear optical effects, including the Kerr effect, self-phase modulation, and four-wave mixing (FWM).
Four-wave mixing (FWM) is a third-order nonlinear optical process in which three photons interact through the medium's nonlinear polarization to generate a fourth photon. The process obeys two fundamental conservation rules: conservation of energy and conservation of momentum (phase matching). These can be written as:

$$\omega_4 = \omega_1 + \omega_2 - \omega_3, \quad \text{and} \quad \vec{k}_4 = \vec{k}_1 + \vec{k}_2 - \vec{k}_3$$

where ω denotes the frequency and k the wave vector of each light wave.

A special and very important case of FWM is *Spontaneous Four-Wave Mixing (SFWM).* In SFWM, two photons from a strong pump field are annihilated within the nonlinear medium, generating a pair of new photons, known as the *signal* and *idler* photons. This occurs spontaneously, without requiring a seed input for the new frequencies. The energy conservation relation for SFWM is:

$$2\omega_p = \omega_s + \omega_i$$

where ω_p is the pump frequency, and ω_s and ω_i are the signal and idler frequencies, respectively.

Caterina Vigliar: catvi@dtu.dk
Mujtaba Zahidy: muzah@dtu.dk
HSOC Group, DTU ELECTRO
Teaching assistants: Damien Roux, Inaki Beraza.

SFWM commonly occurs in optical fibers, waveguides, and integrated photonic devices where the nonlinear susceptibility $\chi^{(3)}$ is significant. Because the signal and idler photons are created simultaneously and share correlated properties such as energy and polarization, SFWM serves as a powerful mechanism for generating *entangled photon pairs* and *single-photon sources* used in quantum communication and quantum information processing.

This pair generation is a *probabilistic quantum process*. When the pump power is low, the probability of creating a single photon pair per pump pulse is very small (typically 10^{-4}–10^{-2}). However, as the pump intensity increases, the nonlinear interaction becomes stronger, and the likelihood of generating *multiple photon pairs* during a single pulse rises significantly. These *multi-photon events* originate from multiple simultaneous SFWM interactions occurring within the same medium. Essentially, more than one pair of signal–idler photons can be produced from the same pump pulse. The quantum state of light produced by SFWM can therefore be written as a *superposition* of vacuum, single-pair, and multi-pair states:

$$|\psi\rangle = |0\rangle + \lambda|1_s, 1_i\rangle + \lambda^2|2_s, 2_i\rangle + \dots$$

where λ is a small parameter proportional to the nonlinear interaction strength and the pump field amplitude. More in detail, for low pump powers, the state produced by the SFWM Hamiltonian acting on the vacuum can be approximated with

$$|\psi\rangle \simeq \left(\mathbb{1} - i\gamma LP \int d\omega_i d\omega_s \mathscr{A}(\omega_i, \omega_s)\hat{a}_i^\dagger(\omega_i)\hat{a}_s^\dagger(\omega_s)\right)|0\rangle_i |0\rangle_s = |0\rangle_i |0\rangle_s + |\psi_{11}\rangle_{i,s},$$

where higher order terms are neglected. In this regime, the process is approximating a probabilistic photon-pair source, emitting a two-photon state

$$|\psi_{11}\rangle_{i,s} = \int d\omega_i d\omega_s \mathscr{A}(\omega_i, \omega_s)|1\rangle_i |1\rangle_s$$

with probability $p = \gamma^2 L^2 P^2$, where γ represents is the non-linear parameter, which depends on the susceptibility and on the light field's mode properties, *L* represents the length of the waveguide and *P* the pump's peak power. Ideal frequency un-correlated photons can be extracted from this process by introducing tight filtering on the output signal and idler fields, enforcing the factorability of the two-photon state.The sources used in the experiment carried ot in this course will be based on this process.

Caterina Vigliar: catvi@dtu.dk
Mujtaba Zahidy: muzah@dtu.dk

HSOC Group, DTU ELECTRO
Teaching assistants: Damien Roux, Inaki Beraza.

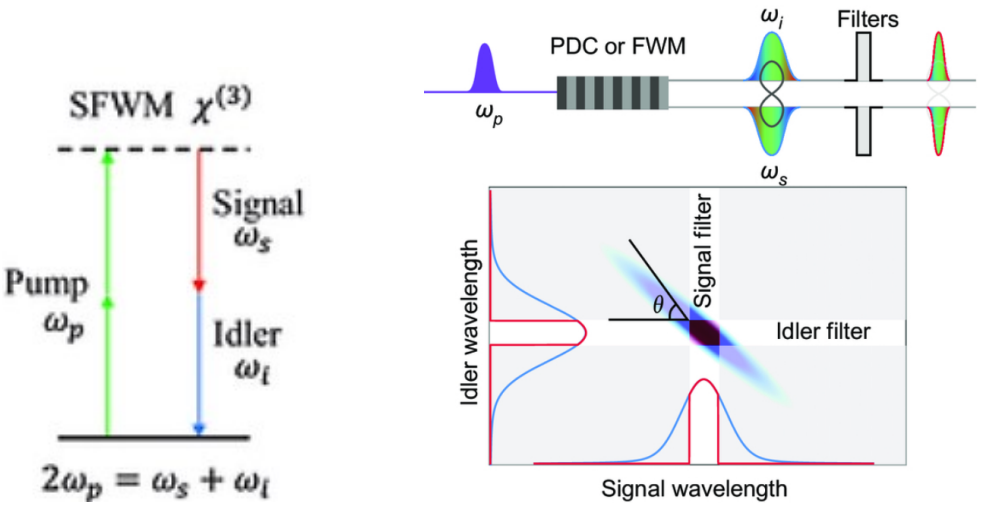

Figure 4: Left: schematic illustrating the SFWM process determined by energy and momentum conservation conditions. In this scheme, two pump photons at the same wavelength (depicted in green) are annihilated, resulting in two photons spontaneously emitted at different frequencies (red and blue), symmetric with respect to the pump frequency. Right: Photon pair generation and narrowband filtering, with corresponding joint spectral intensity spectrum of signal and idler photons [18]. Figure from Physical Review A, Evan Meyer-Scott et al., American Physical Society, 2017.

Large-scale integrated optical circuits: entanglement generation and measurement

Entangled pairs of photons can be post-selected by coherently pumping two sources, selecting the case where one photon pair is generated in a superposition between the two sources. The circuit is shown in Fig. 5: two parallel SFWM sources produce two pairs that can be spatially routed by asymmetric Mach-Zehnders into four modes defining two path-encoded qubits: signal qubit (s) and idler qubit (i). If we look at the unnormalised state produced by the two SFWM sources in the Fock basis we obtain

$$|\psi\rangle = |0000\rangle_{s_0 s_1 i_0 i_1} + \eta |1010\rangle_{s_0 s_1 i_0 i_1} + \eta |0101\rangle_{s_0 s_1 i_0 i_1} + \eta^2 |2020\rangle_{s_0 s_1 i_0 i_1} + \eta^2 |0202\rangle_{s_0 s_1 i_0 i_1} + \ldots,$$

where the modes are ordered so that signal photons come before idler photons, and pedices indicate the dual-rail qubit modes. We can see that, if we restrict to only one photon pair generation, this is equivalent to the Bell pair

$$|\phi^+\rangle = |00\rangle_{si} + |11\rangle_{si}$$

in the qubit basis. When we place a beam splitter on the path of each dual-rail qubit we erase the information about which source fired, enabling quantum state superposition. The state is *post-selected* by the detection of coincidences of one photon in the space of each qubit. This entanglement generation scheme cen be extended by placing many of these sources in parallel. With similar post-selection principles can post-select entangled bi-partite d-dimensional path encoded systems [19] or even multi-partite path-encoded entangled states [20].

Caterina Vigliar: catvi@dtu.dk
Mujtaba Zahidy: muzah@dtu.dk

HSOC Group, DTU ELECTRO
Teaching assistants: Damien Roux, Inaki Beraza.

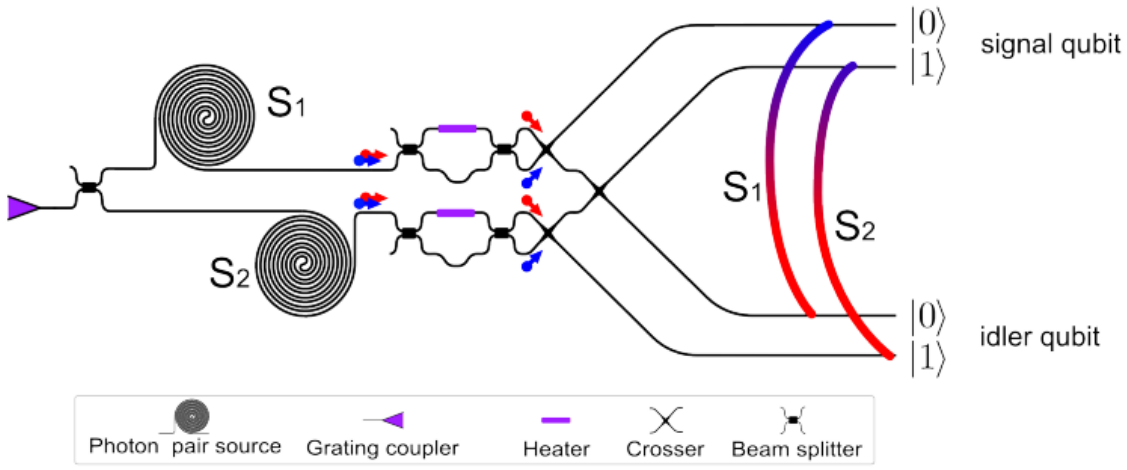

Figure 5: ***Bell pair generation with integrated optics.*** *Interferometer used to realise a Bell pair* $|\psi\rangle = |00\rangle_{si} + |11\rangle_{si}$ *in post-selection. Two non-degenerate signal and idler photons, indicated in blue and red and generated in a superposition over two spiral sources, encode one qubit each.*

Caterina Vigliar: catvi@dtu.dk
Mujtaba Zahidy: muzah@dtu.dk

HSOC Group, DTU ELECTRO
Teaching assistants: Damien Roux, Inaki Beraza.

The IQIS course experimental setup

An overview of the experimental setup and available equipment is shown in Fig. 6.

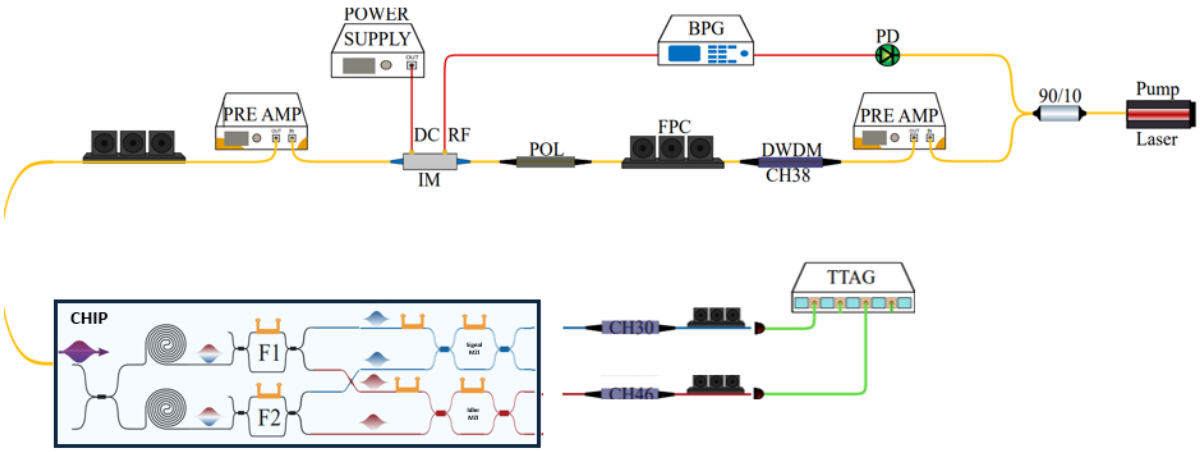

Figure 6: Experiment schematic for the Silicon/Silicon Nitride setup.

For ease of explanation the experimental experience can be divided into five different parts: (A) photonic building blocks characterization, (B) pulsed laser source characterization, (C) spontaneous four-wave mixing source characterization, (D) two-qubit Bell-state quantum state tomography experiment and (E) data collection and analysis.

Caterina Vigliar: catvi@dtu.dk
Mujtaba Zahidy: muzah@dtu.dk

HSOC Group, DTU ELECTRO
Teaching assistants: Damien Roux, Inaki Beraza.

PART A - Photonic building blocks characterization

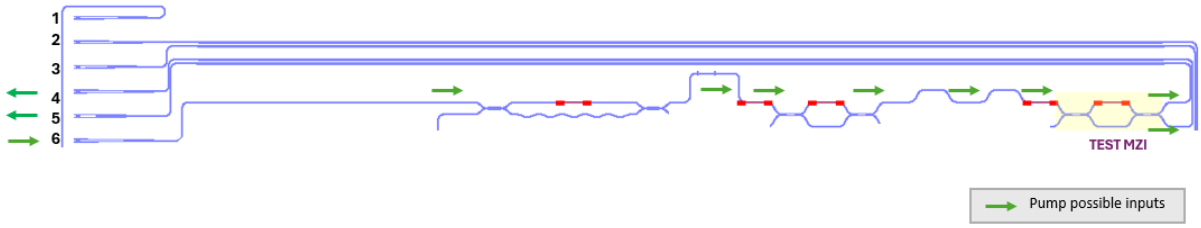

Figure A1: *Integrated Mach-Zehnder building blocks that can be analysed in the Silicon Setup.*

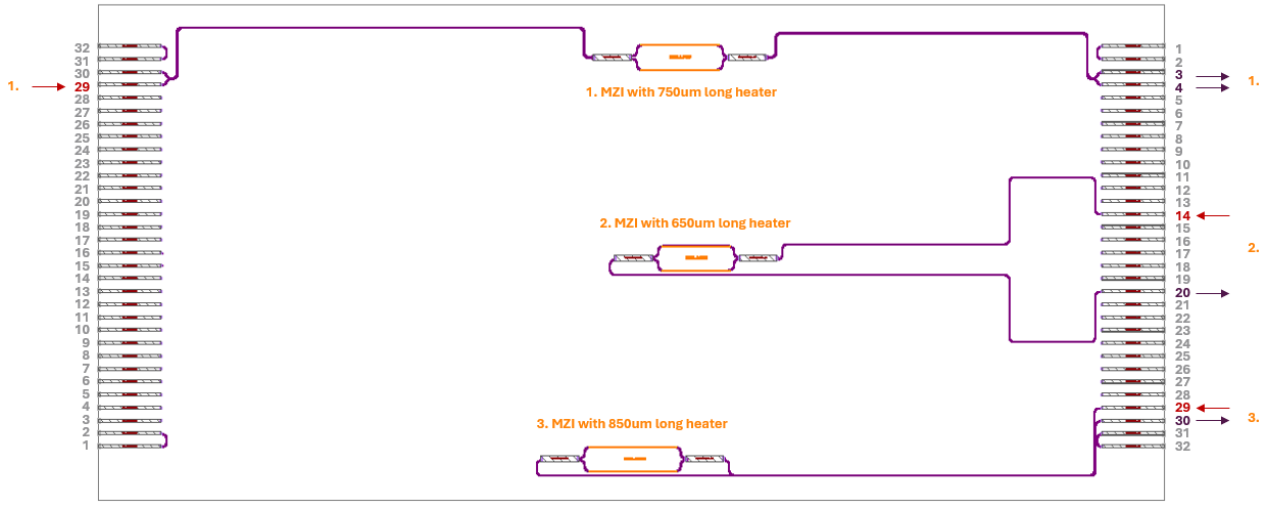

Figure A2: *Integrated Mach-Zehnder building blocks that can be analysed in the Silicon Nitride Setup. Red arrows indicate possible laser light inputs. Purple arrows represents possible light collection outputs.*

Mach-Zehnder Interferometers

As descripted in the introduction section, also the integrated devices under test in this IQIS lab experience can be reconfigured by thermo-optic phase shifters places within Mach-Zehnders interferometers. Each phase shifter has a particular voltage-phase nonlinear relation due to variations in the fabrication process, therefore each heater has to be individually characterised. Waveguides are strategically placed around the device to allow independent calibration of each on-chip phase shifter. Here we are going to characherize one as a sample of the many you will use for the tomography experiment. We perform this calibration in two steps. We first perform current-voltage curves for all the heaters, taking into account deviations form the ideal linear case, mainly due to a non-ohmic behaviour as the temperature changes. We fit the data with

$$I(V) = \rho_0 + \rho_1 V + \rho_2 V^2$$

obtaining therefore the power-voltage relation, through three resistance parameters

$$P(V) = VI = V(\rho_0 + \rho_1 V + \rho_2 V^2).$$

Secondly, we scan the heater's voltage to perform a bright-light optical fringe, collecting the optical power transmitted though one port of an MZI including the heater we want to calibrate, independently from all the other heaters. The intensity of the collected light depends on the heater's dissipated power with the following relation:

$$P_{opt}(P) = (B + A) - A\cos(\omega P - \phi_0),$$

where $\phi = \omega P - \phi_0$ is the effective phase applied in the MZI. By fitting the classical fringe data with the above function we obtain ω and ϕ that allow us to completely reconstruct the phase-voltage relation:

$$\phi(V) = \omega P(V) - \phi_0 = -\phi_0 + \omega(\rho_0 V + \rho_1 V^2 + \rho_2 V^3).$$

In this process average classical visibilities of 98% are observed. Examples of this curves are reported in Fig. A3.

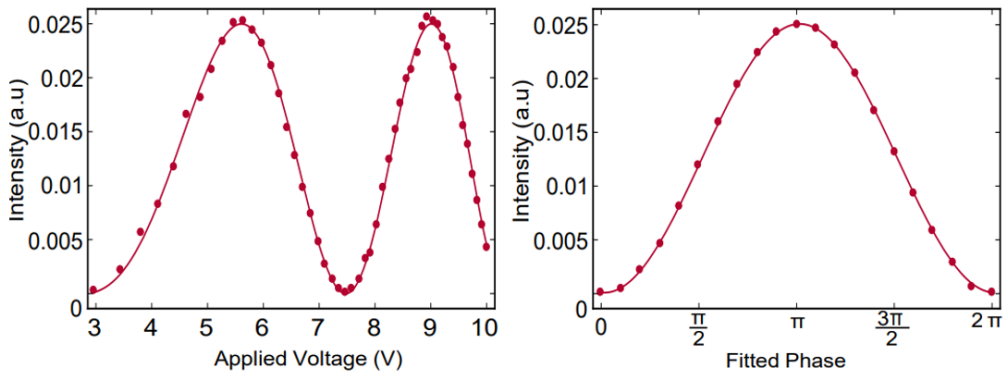

Figure A3: *Thermo-optic phase shifters' typical characterisation fringes. The insets show an MZI optical fringe as a function of the applied voltage and of the derived phase.*

In the lab: for the Silicon setup

Reconfigure the setup to isolate a single Mach-Zehnder as in Fig. A1. Using CW classical light, perform a voltage sweep of the phase shifter and observe the electrical and optical response. Plot the interference fringe and extract the relevant Mach-Zehnder calibration parameters: offset-phase, period, and visibility.

In the lab: for the Silicon nitride setup

Find one isolated single Mach-Zehnder among the ones highlighted in Fig.A2 and identify input/output ports on the fiber arrays. Using CW classical light, perform a voltage sweep of the phase shifter and

observe the electrical and optical response. Plot the interference fringe and extract the relevant Mach-Zehnder calibration parameters: offset-phase, period, visibility.

EXERCISE – PART A: Discuss the procedure on how to extract the voltage to apply, given a pre-selected phase. For which phase/voltage settings the light gets completely transmitted (Identity, 100:0), totally deflected (swap, 0:100) or split in half (balanced beam-splitter, 50:50)? Verify the voltage values found by collecting light from the relative output ports.

PART B- Pulsed laser source characterization

In the introduction section, we introduced one type of third-order interaction: four-wave mixing. This specific interaction, as well as many others, depends on the intensity of the electromagnetic waves involved. While the dependence can be of any order, linear, quadratic or else, the interaction always grows stronger with the intensity of light due to the presence of a stronger field. In this section, we introduce a method of generating high-power short duty-cycle laser pulses for applications such as photon-pair generation via FWM. Please note that this introductory section has been simplified, and the references are given for interested readers.

B.1 Continuous-Wave (CW) light vs pulsed laser:

Before we continue, we need to understand the difference between a continuous-wave (CW) laser, and a pulsed laser. Ideally, a laser is a *monochromatic* or single-frequency electromagnetic wave, whose electric field in its most simple form as a function of space and time, can be described as

$$\vec{E}(z,t) = E_0 \cos(kz - 2\pi f t).$$

where E_0 is the amplitude of the electric field, k is the wave vector and f is the frequency. The intensity of the light corresponds to the square of the amplitude: $I \propto |E_0|^2$

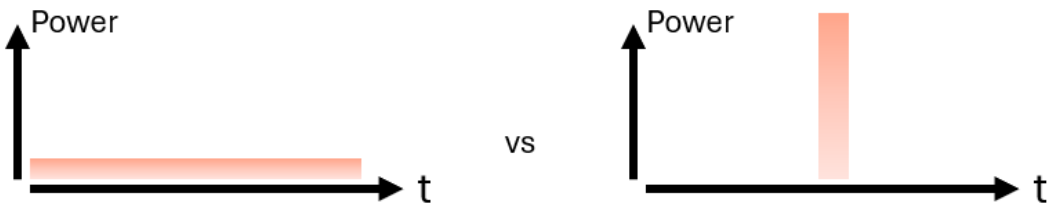

Figure B1: A laser's optical power in CW and pulsed regimes.

A characteristic of CW light is constant energy – or power – over any window of time. For many applications, such as the generation of photon pairs through SFWM, it is necessary to concentrate all that energy in a short period of time, to achieve higher intensities, therefore a stronger SFWM effect in the material.

Caterina Vigliar: catvi@dtu.dk
Mujtaba Zahidy: muzah@dtu.dk

HSOC Group, DTU ELECTRO
Teaching assistants: Damien Roux, Inaki Beraza.

REFLECTION: *The intensity of light at a location z_0, corresponds to the square of the field's amplitude.*

$$I \propto E_0^2 \cos^2(kz_0 - 2\pi ft).$$

which is a trigonometric function oscillating between 0 and E_0^2. However, since the frequency of light is very high, for example, for red light it is about 450 THz or 450 million million Hz, it is perceived as the average of that oscillation. A useful mathematical identity is

$$2\pi \int_0^T \cos^2(kz_0 - 2\pi ft) = \frac{1}{2}$$

This equation translates into the intensity of light being perceived as constant for measurement tools, or human eyes.

One way to achieve pulsed laser light, is through a teachnique called *mode-locking*. To understand this technique we need to first go through some basic principles of light *interference* and the concept of light *modes*.

B.2 Interference basics

Interference is the phenomenon that occurs when two or more waves overlap in space and time, resulting in a new wave pattern formed by the superposition of their electric (or other) field amplitudes. Here are examples of two cosine waves superposed with different phase differences.

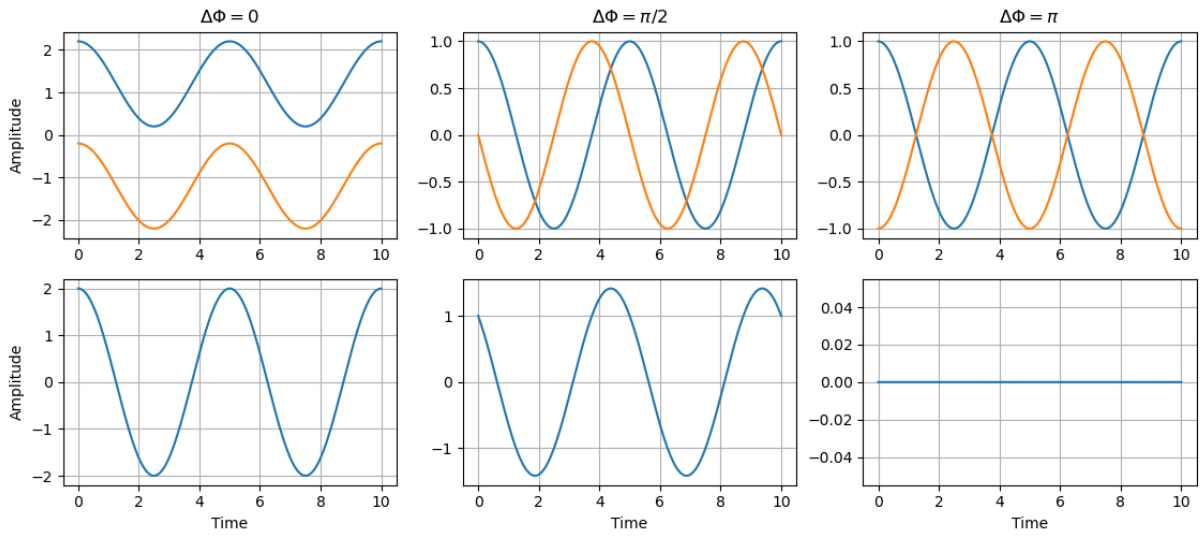

Figure B2: *Interference examples: top row represents two original light fields, bottom row corresponds to the resulting sum of the two above.*

Perhaps, a physical example known to many is Young's double slit experiment. The spatial superposition of two waves from two slits creates fringes which express as bright and dark lines on a screen. Note that in the interference process, the total energy is constant, however, it is concentrated in bright lines.

Caterina Vigliar: catvi@dtu.dk
Mujtaba Zahidy: muzah@dtu.dk

HSOC Group, DTU ELECTRO
Teaching assistants: Damien Roux, Inaki Beraza.

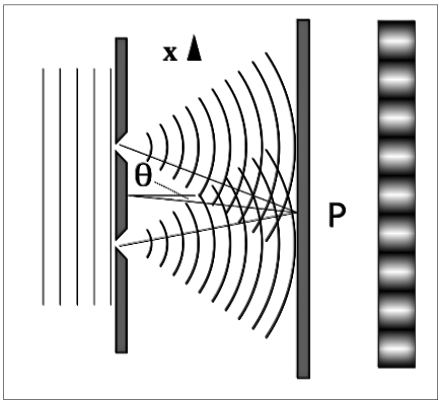

Figure B3: Young's double slit experiment.

B.3 The concept of light modes

Regarding the concept of *modes* of light. Perhaps, the easiest way to demonstrate this is for acoustic waves appearing in guitar strings. In the presence of boundary conditions, only a subset of frequencies is physically acceptable. For instance, in the case of guitar strings, since the two ends are fixed, the acceptable vibrational modes, also known as standing waves, can be depicted as below:

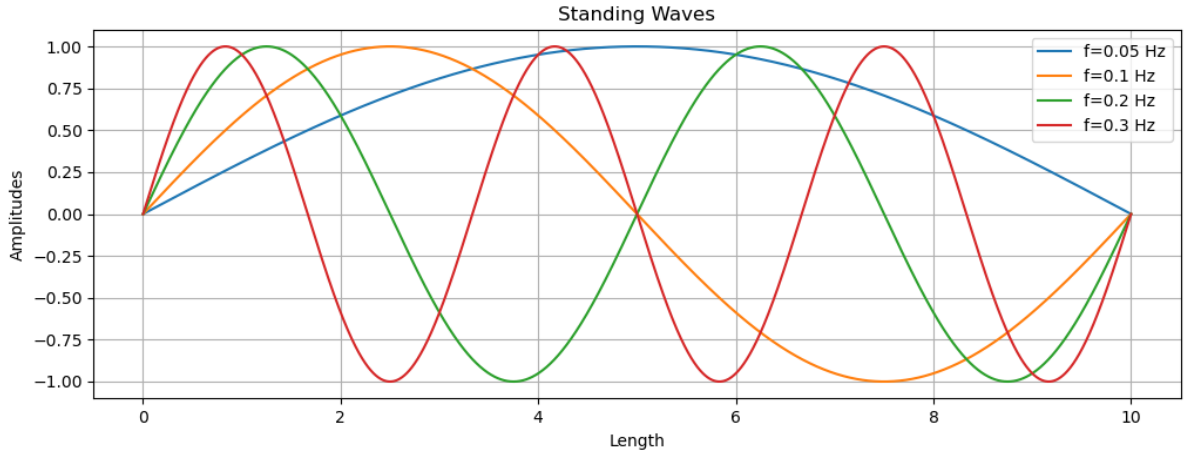

Figure B4: Standing waves examples.

The wavelength of a given mode *n* is $\lambda_n = \frac{2L}{n}$.

Similarly to acoustic waves on a guitar, light waves can be trapped in a region formed by two mirrors, called an optical cavity or resonator. For a cavity of length *L*, the allowed frequencies are $f_m = \frac{mc}{2L}$ where the cavity supports a set of equally spaced frequencies given by cavity's free spectral range (FSR):

$$\Delta f = f_{m+1} - f_m = \frac{c}{2L}$$

Now, let's see what happens if we add up a number of equi-spaced waves with each other:

Caterina Vigliar: catvi@dtu.dk
Mujtaba Zahidy: muzah@dtu.dk

HSOC Group, DTU ELECTRO
Teaching assistants: Damien Roux, Inaki Beraza.

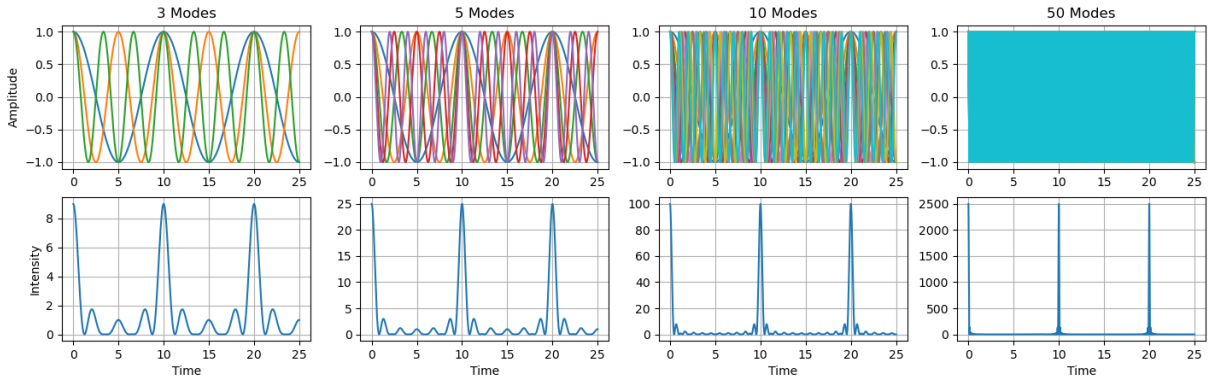

Figure B5: *Mode-locking examples.*

In the example above, waves of frequencies *f=0.1*m* are added. As can be seen, the more modes are added to each other, the eventual field becomes more concentrated, leading to extremely short pulses. The pulse width can be estimated by

$$\tau_p \approx \frac{1}{N\Delta f}$$

where *N* is the number of modes participating in the formation of the pulse. Note that in the example above, all the modes start from the same point (i.e. same phase), hence the name mode-locking. If we add some phase noise to the modes, the final field will become distorted:

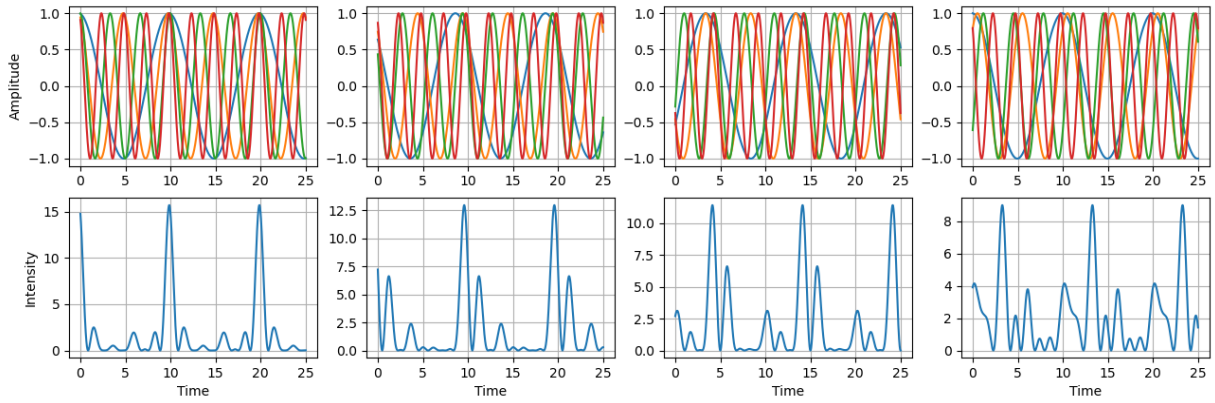

Figure B6: *Examples of distorted mode-locking with random noise.*

Here, a progressively random phase is added to the 4 modes contributing to the final field. As you can see, the more noise is added, the stronger the distortion. The relation between the peak power of the pulse and energy of the pulse is given by:

$$P_{Peak} = \cosh^{-1}(\sqrt{2})\frac{E_{Pulse}}{T} \approx 0.88\frac{E_{Pulse}}{T}$$

where T is the pulse full width at half of its maximum (FWHM).

EXERCISE – PART B: Discuss the procedure on how to estimate the pulse width of a given pulsed laser looking at its spectrum from an optical spectrum analyser (OSA). Estimate the peak power having average power and repetition rate.

Caterina Vigliar: catvi@dtu.dk
Mujtaba Zahidy: muzah@dtu.dk

HSOC Group, DTU ELECTRO
Teaching assistants: Damien Roux, Inaki Beraza.

PART C - Spontaneous four-wave mixing source characterization

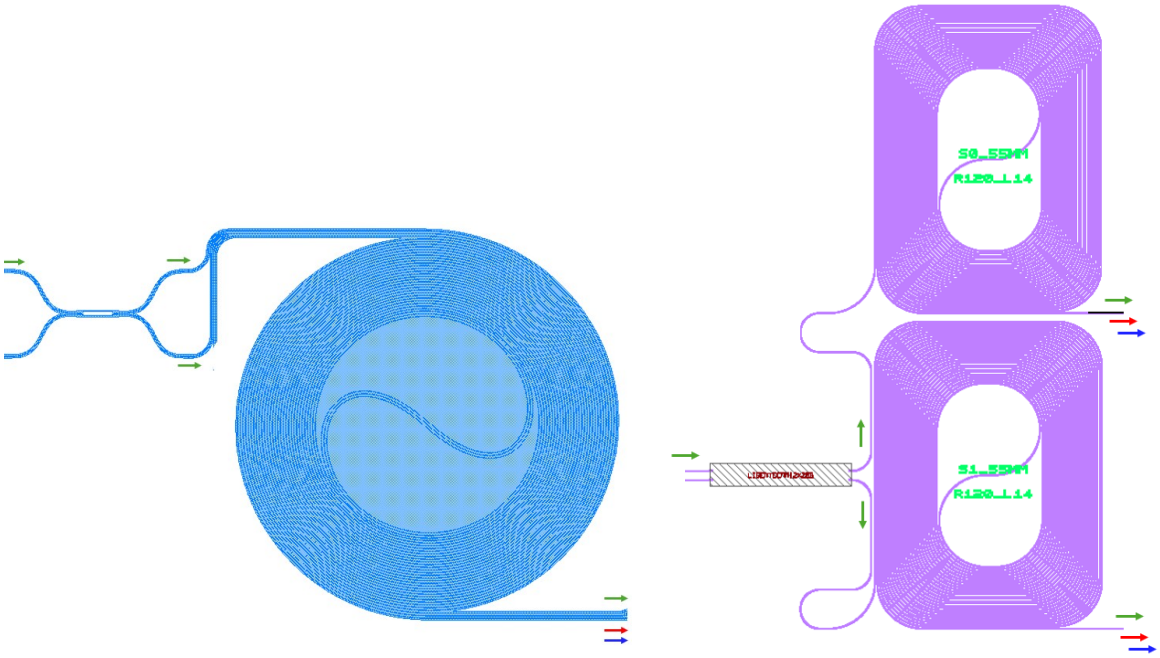

Figure C1: *Zoomed-in schematics of spontaneous-four wave mixing sources based on Silicon (left) Silicon Nitride (right) spiral waveguides that can be analysed in the two IQIS setups. Green arrows indicate laser light inputs. Blue and red arrows represent spontaneously generated signal and idler light fields.*

Once the device's active components are characterised, preliminary tests on the photon-pair sources can be performed. In our chips two 1.5-cm-long spiral silicon waveguides are present (Silicon setup) or two 5.5-cm-long spiral silicon nitride waveguides are present (Silicon Nitride setup) . In these spirals, bright telecommunications-band pump pulses are converted into quantum-correlated signal and idler photons through spontaneous four-wave mixing (see introduction section for more details). In order to verify that each source works individually we isolate one spiral and measure the rate of two-photon coincidences whilst changing the launched power, finding a quadratic relationship that confirms the presence of a third-order non-linear process (spontaneous four-wave mixing or SFWM in short) – see Fig. C2.A.

To estimate the photon pair generation rate *p*, i.e. the probability of each pulse to generate one or more photon pairs, we use a coupling-independent metric. By assuming the coincidences and singles rates to be

$$C = \eta_s \eta_i R \text{ and } S_s = \eta_s R,\ S_i = \eta_i R,$$

where η_s and η_i are the signal and idler transmissions, and C and S_s, S_i are the coincidence and singles rates, the ratio between the product of the singles and the coincidence rates gives an estimate of *R*. Dividing then *R* by the laser's repetition rate we obtain *p* . Values of photon pair generation rates for similar silicon sources at different input powers are shown in Fig. C2.B.

Caterina Vigliar: catvi@dtu.dk
Mujtaba Zahidy: muzah@dtu.dk

HSOC Group, DTU ELECTRO
Teaching assistants: Damien Roux, Inaki Beraza.

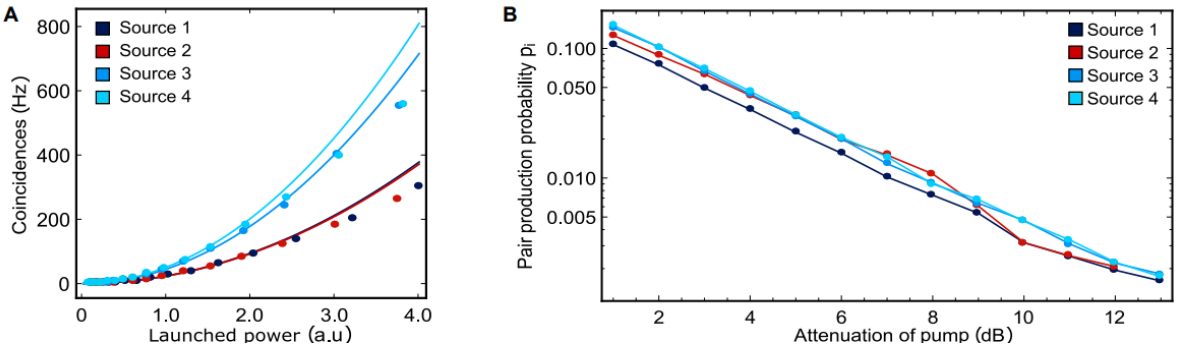

Figure C2: Examples of sources characterisation in the two-qubit Bell-state device. A. Coincidences rates for the various photon pair sources present. B. Probability of generating at least one photon pair as a function of pump attenuation.

In the lab: for the Silicon and Silicon Nitride setups

In the Quantum Lab, using a 1.5-cm long silicon spiral waveguide appropriately pumped and filtered, you will see single photon detection clicks - a result of a spontaneous four-wave mixing process. Photons generated on chip are sent to superconducting single photon detectors located in the adjacent detector room, to which we have optical fibre connection. Single and coincident photon counts are recorded with high-fidelity through a time tagger and are displayed through its relative software.

Discuss the observed number of singles and coincidence clicks on signal and idler channels collecting light from a single spiral source. Collect data (singles and coincidences) for at least four different input powers. Verify the quadratic trend by plotting the data, similarly to Fig. C2. Estimate the generation probability *p*. Discuss what is the *heralding efficiency*.

Observe the histogram of the coincident clicks' arrival times.

EXERCISE – PART C: What is the expected trend of the histogram? Why do we see peaks? Why are the peaks of different height? What can we extract from the relative height between the central main peak and the side peaks? Compare the extracted quantity to another one extracted before though another method.

Caterina Vigliar: catvi@dtu.dk
Mujtaba Zahidy: muzah@dtu.dk

HSOC Group, DTU ELECTRO
Teaching assistants: Damien Roux, Inaki Beraza.

PART D - Two-qubit Bell-state quantum state tomography experiment

D.1 Bell-state generation – realization in silicon and silicon nitride

The diagrams below show how to realize Bell state $|\psi\rangle = |00\rangle_{si} + |11\rangle_{si}$ generation in post-selection with a silicon or silicon nitride chips.

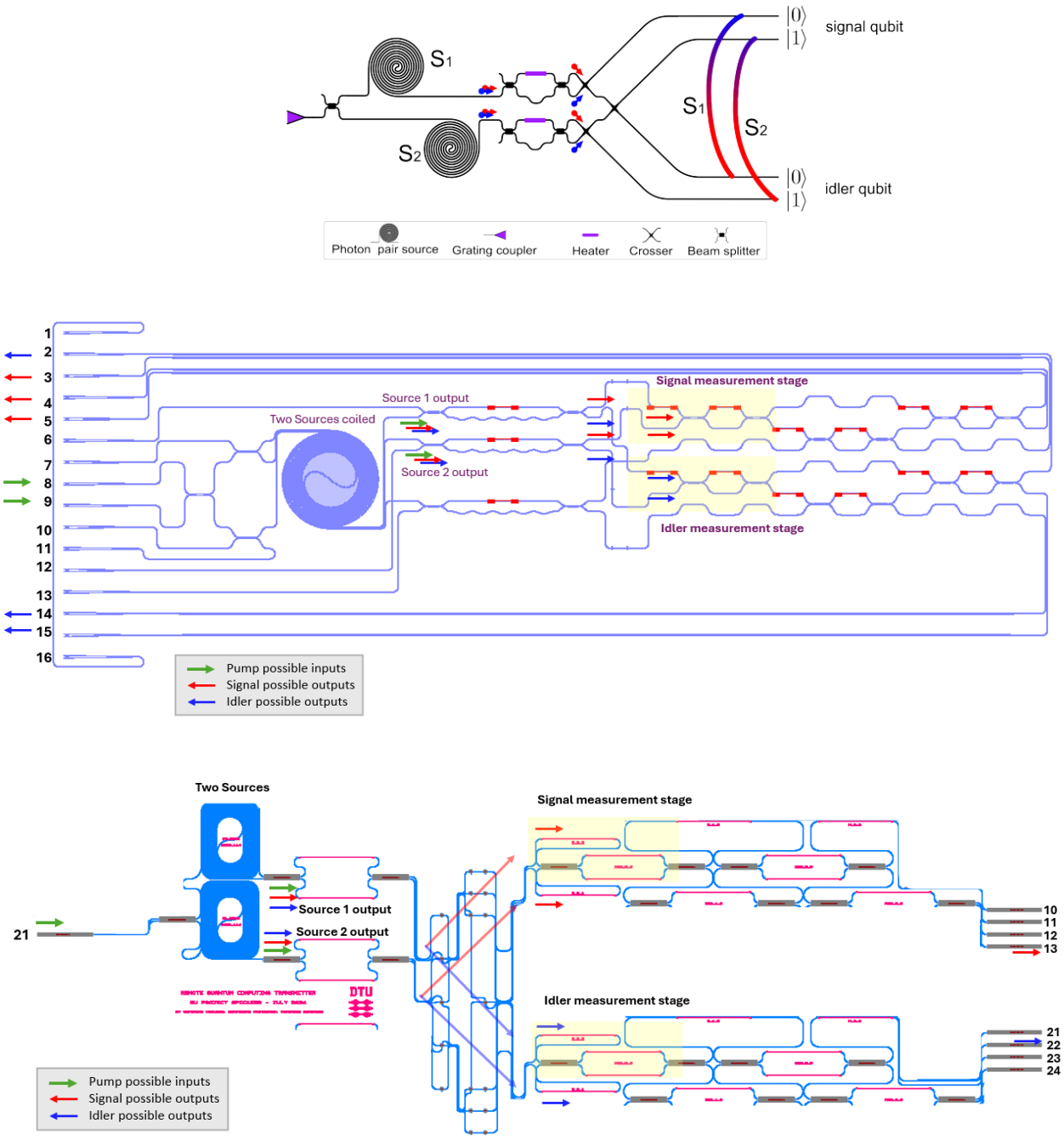

Figure D1: Diagram of the Bell-state generation circuit (top) and its physical implementation in on a silicon device (middle) and on a silicon nitride device (bottom). Waveguides, crossings and beam-splitters are represented with blue lines, while heaters in red. Red and blue arrows represent possible signal and idler light paths.

Caterina Vigliar: catvi@dtu.dk
Mujtaba Zahidy: muzah@dtu.dk

HSOC Group, DTU ELECTRO
Teaching assistants: Damien Roux, Inaki Beraza.

D.2 Full two-qubit quantum state tomography: measurement settings

One of the possible ways to reconstruct a two-qubit density matrix is by performing a state tomography based on Pauli operators' projective measurements:

$$\hat{\mathbf{I}} = \begin{pmatrix} 1 & 0 \\ 0 & 1 \end{pmatrix}, \quad \hat{X} = \begin{pmatrix} 0 & 1 \\ 1 & 0 \end{pmatrix}, \quad \hat{Y} = \begin{pmatrix} 0 & -i \\ i & 0 \end{pmatrix} \quad \hat{Z} = \begin{pmatrix} 1 & 0 \\ 0 & -1 \end{pmatrix}.$$

A projective measurement using the Pauli operators above, corresponds to measuring the state in each Pauli operator's specific eigenbasis, which effectively collapses the state of the system to an eigenstate of the operator. For example, a measurement in the Z basis corresponds to measuring the state in the computational basis ($|0\rangle$, $|1\rangle$). To collapse the state into a specific state of a given eigenbasis, we use Mach-Zehnder interferometers and single photon detectors placed in front of one of its output paths.

Following the details provided in the background section, Mach-Zehnder interferometers can be used to manipulate the interference between two paths of light. They therefore allow to rotate any initial quantum state, inputted across its two input modes, into arbitrary quantum states represented by its two output modes, by applying a set of phase values $(\varphi, \phi_1, \phi_2)$.

$$\hat{U}(2) = \hat{R}_Z(\gamma)\hat{R}_Y(\beta)\hat{R}_Z(\alpha) = \hat{U}_{PS}(\phi_2)\hat{U}_{MZI}(\varphi)\hat{U}_{PS}(\phi_1)$$

EXERCISE 1 – PART D: given the Pauli operators definitions above and the derivation of an arbitrary unitary realised by phase shifters and beamsplitters in an MZI which dependent on $(\varphi, \phi_1, \phi_2)$, find the phase values that correspond projecting an arbitrary state $|\psi\rangle = a|0\rangle + b|1\rangle$ on the Z and X eigenbasis.

The outcome probability of each projective measurement can be extracted by counting the number of photons arriving in a pre-determined time window across the two modes.

In the lab: for the Silicon and Silicon Nitride setups

1. Identify a possible input port for pumping two spiral sources simultaneously, and identify the corresponding number on the fiber array by looking at the circuit under the microscope.
2. Identify possible output ports for collecting signal and idler light and the corresponding fiber number on the fiber array.
3. Connect output filters for signal and idler channels and finally the fibers leading to single photon detection.
4. Apply phase settings corresponding to projecting the created state into the ZZ basis.
5. Adjust optical and electrical delays to synchronize the arrival times of the photons on the time tagger device and observe the singles, coincident counts and histogram of the photons' arrival time for all the ZZ basis measurement settings. Verify we are in a regime where the generation probability *p* is close to 3%.

Caterina Vigliar: catvi@dtu.dk
Mujtaba Zahidy: muzah@dtu.dk

HSOC Group, DTU ELECTRO
Teaching assistants: Damien Roux, Inaki Beraza.

EXERCISE 2 – PART D: Write the generated state $|\psi\rangle = |00\rangle_{si} + |11\rangle_{si}$ in the XX basis. Observe coincidence counts also in the XX basis measurements. Discuss the observed outcomes. Do the observed probabilities match the expectations? If not, why? Do the same for YY measurement settings.

D.3 Tomography reconstruction

The expectation values of all the two-qubit combinations of Pauli operators can be obtained in the following way, starting from the four two-qubit projective measurements composing each of them.

$$
\begin{aligned}
\langle IZ\rangle &= \langle 00|ZZ|00\rangle - \langle 01|ZZ|01\rangle + \langle 10|ZZ|10\rangle - \langle 11|ZZ|11\rangle \\
\langle ZI\rangle &= \langle 00|ZZ|00\rangle + \langle 01|ZZ|01\rangle - \langle 10|ZZ|10\rangle - \langle 11|ZZ|11\rangle \\
\langle ZZ\rangle &= \langle 00|ZZ|00\rangle - \langle 01|ZZ|01\rangle - \langle 10|ZZ|10\rangle + \langle 11|ZZ|11\rangle \\
\\
\langle IX\rangle &= \langle 00|ZX|00\rangle - \langle 01|ZX|01\rangle + \langle 10|ZX|10\rangle - \langle 11|ZX|11\rangle \\
\langle XI\rangle &= \langle 00|XZ|00\rangle + \langle 01|XZ|01\rangle - \langle 10|XZ|10\rangle - \langle 11|XZ|11\rangle \\
\langle XX\rangle &= \langle 00|XX|00\rangle - \langle 01|XX|01\rangle - \langle 10|XX|10\rangle + \langle 11|XX|11\rangle \\
\\
\langle IY\rangle &= \langle 00|ZY|00\rangle - \langle 01|ZY|01\rangle + \langle 10|ZY|10\rangle - \langle 11|ZY|11\rangle \\
\langle YI\rangle &= \langle 00|YZ|00\rangle + \langle 01|YZ|01\rangle - \langle 10|YZ|10\rangle - \langle 11|YZ|11\rangle \\
\langle YY\rangle &= \langle 00|YY|00\rangle - \langle 01|YY|01\rangle - \langle 10|YY|10\rangle + \langle 11|YY|11\rangle \\
\\
\langle ZX\rangle &= \langle 00|ZX|00\rangle - \langle 01|ZX|01\rangle - \langle 10|ZX|10\rangle + \langle 11|ZX|11\rangle \\
\langle ZY\rangle &= \langle 00|ZY|00\rangle - \langle 01|ZY|01\rangle - \langle 10|ZY|10\rangle + \langle 11|ZY|11\rangle \\
\\
\langle XZ\rangle &= \langle 00|XZ|00\rangle - \langle 01|XZ|01\rangle - \langle 10|XZ|10\rangle + \langle 11|XZ|11\rangle \\
\langle XY\rangle &= \langle 00|XY|00\rangle - \langle 01|XY|01\rangle - \langle 10|XY|10\rangle + \langle 11|XY|11\rangle \\
\\
\langle YX\rangle &= \langle 00|YX|00\rangle - \langle 01|YX|01\rangle - \langle 10|YX|10\rangle + \langle 11|YX|11\rangle \\
\langle YZ\rangle &= \langle 00|YZ|00\rangle - \langle 01|YZ|01\rangle - \langle 10|YZ|10\rangle + \langle 11|YZ|11\rangle \\
\\
\langle II\rangle &= \langle 00|ZZ|00\rangle + \langle 01|ZZ|01\rangle + \langle 10|ZZ|10\rangle + \langle 11|ZZ|11\rangle
\end{aligned}
$$

The different Pauli operator expectation values contribute to the components of the density matrix in the following way:

$$
\rho = \frac{1}{4}\begin{bmatrix}
\langle II\rangle + \langle IZ\rangle + \langle ZI\rangle + \langle ZZ\rangle & \langle IX\rangle - i\langle IY\rangle + \langle ZX\rangle - i\langle ZY\rangle & \langle XI\rangle + \langle XZ\rangle - i\langle YI\rangle - i\langle YZ\rangle & \langle XX\rangle - i\langle XY\rangle - i\langle YX\rangle - \langle YY\rangle \\
\langle IX\rangle + i\langle IY\rangle + \langle ZX\rangle + i\langle ZY\rangle & \langle II\rangle - \langle IZ\rangle + \langle ZI\rangle - \langle ZZ\rangle & \langle XX\rangle + i\langle XY\rangle - i\langle YX\rangle + \langle YY\rangle & \langle XI\rangle - \langle XZ\rangle - i\langle YI\rangle + i\langle YZ\rangle \\
\langle XI\rangle + \langle XZ\rangle + i\langle YI\rangle + i\langle YZ\rangle & \langle XX\rangle - i\langle XY\rangle + i\langle YX\rangle + \langle YY\rangle & \langle II\rangle + \langle IZ\rangle - \langle ZI\rangle - \langle ZZ\rangle & \langle IX\rangle - i\langle IY\rangle - \langle ZX\rangle + i\langle ZY\rangle \\
\langle XX\rangle + i\langle XY\rangle + i\langle YX\rangle - \langle YY\rangle & \langle XI\rangle - \langle XZ\rangle + i\langle YI\rangle - i\langle YZ\rangle & \langle IX\rangle + i\langle IY\rangle - \langle ZX\rangle - i\langle ZY\rangle & \langle II\rangle - \langle IZ\rangle - \langle ZI\rangle + \langle ZZ\rangle
\end{bmatrix}
$$

The fidelity between the reconstructed density matrix and the ideal quantum state, expressed by the density matrix σ, is commonly defined as:

$$
F(\rho,\sigma) = \left(\mathrm{tr}\sqrt{\sqrt{\rho}\sigma\sqrt{\rho}}\right)^2
$$

Caterina Vigliar: catvi@dtu.dk
Mujtaba Zahidy: muzah@dtu.dk

HSOC Group, DTU ELECTRO
Teaching assistants: Damien Roux, Inaki Beraza.

In the lab for all students

1. Apply the full set of measurement settings given to perform the full state tomography of a two-qubit Bell state. Discuss the measurement procedure and agree on necessary integration times, depending on the observed rates.
2. Collect data from the provided SNSPDs interface and software for each given projective measurement. Save in a shared folder for subsequent data analysis.
3. Discuss the procedure on how to reconstruct the density matrix from the full set of projective measurements.

PART E - Data analysis

Data analysis

Given the full set of preliminary source characterization data and tomographic projective measurement results:

1. Plot histogram of the single and idler photons arrival times for a 3% generation probability from the silicon waveguide sample or the silicon nitride sample.
2. Estimate pair generation rate given the above histogram.
3. Estimate heralding efficiency given the coincidences and single counts from the ZZ measurements.
4. Extract the number of coincidence (two-fold) clicks for each measurement setting.
5. Calculate the outcome probabilities for each two-qubit operator measured.
6. Reconstruct and plot the Bell-state density matrix (real and imaginary parts or mod and phase).
7. Calculate quantum state fidelity with the expected quantum state.
8. Evaluate and list the most realistic sources of noise that can cause degradation in the state's fidelity. Plot the collected MZI classical optical fringes if necessary.

Poster output

Display the obtained results in an organized and self-explanatory manner. Include some theoretical details, mention of the motivation and experimental challenges. Preferably work in sub-groups not larger than 4 people.

Caterina Vigliar: catvi@dtu.dk
Mujtaba Zahidy: muzah@dtu.dk

HSOC Group, DTU ELECTRO
Teaching assistants: Damien Roux, Inaki Beraza.

REFERENCES:

[1] D. P. DIVINCENZO, The physical implementation of quantum computation, Fortschritte der Physik: Progress of Physics, 48 (2000), pp. 771–783
[2] J. I. CIRAC AND P. ZOLLER, Quantum computations with cold trapped ions, Physical review letters, 74 (1995), p. 4091.
[3] A. M. STEANE, The ion trap quantum information processor, arXiv preprint quantph/9608011, (1996).
[4] L. CHILDRESS AND R. HANSON, Diamond nv centers for quantum computing and quantum networks, MRS bulletin, 38 (2013), pp. 134–138.
[5] Y. MAKHLIN, G. SCHÖN, AND A. SHNIRMAN, Quantum-state engineering with Josephson-junction devices, Reviews of modern physics, 73 (2001), p. 357.
[6] V. ANANT, A. J. KERMAN, E. A. DAULER, J. K. YANG, K. M. ROSFJORD, AND K. K. BERGGREN, Optical properties of superconducting nanowire single-photon detectors, Optics express, 16 (2008), pp. 10750–10761.
[7] C. GERRY AND P. KNIGHT, Introductory quantum optics, Cambridge university press, 2005.
[8] M. RECK, A. ZEILINGER, H. J. BERNSTEIN, AND P. BERTANI, Experimental realization of any discrete unitary operator, Physical review letters, 73 (1994), p. 58.
[9] J. CAROLAN, C. HARROLD, C. SPARROW, E. MARTÍN-LÓPEZ, N. J. RUSSELL, J. W. SILVERSTONE, P. J. SHADBOLT, N. MATSUDA, M. OGUMA, M. ITOH, ET AL., Universal linear optics, Science, 349 (2015), pp. 711–716.
[10] E. KNILL, R. LAFLAMME, AND G. J. MILBURN, A scheme for efficient quantum computation with linear optics, nature, 409 (2001), pp. 46–52.
[11] S. SCHEEL, K. NEMOTO, W. J. MUNRO, AND P. L. KNIGHT, Measurement-induced nonlinearity in linear optics, Physical Review A, 68 (2003), p. 032310.
[12] M. GIMENO-SEGOVIA, P. SHADBOLT, D. E. BROWNE, AND T. RUDOLPH, From three-photon Greenberger-Horne-Zeilinger states to ballistic universal quantum computation, Phys. Rev. Lett., 115 (2015), p. 020502.
[13] W. S. C. CHANG, Fundamentals of guided-wave optoelectronic devices, Cambridge University Press, 2009.
[14] G. LIFANTE, Integrated photonics: fundamentals, John Wiley & Sons, 2003.
[15] J. W. SILVERSTONE, D. BONNEAU, K. OHIRA, N. SUZUKI, H. YOSHIDA, N. IIZUKA, M. EZAKI, C. M. NATARAJAN, M. G. TANNER, R. H. HADFIELD, ET AL., On-chip quantum interference between silicon photon-pair sources, Nature Photonics, 8 (2014), pp. 104—-108.
[16] J. W. SILVERSTONE, R. SANTAGATI, D. BONNEAU, M. J. STRAIN, M. SOREL, J. L. O'BRIEN, AND M. G. THOMPSON, Qubit entanglement between ring-resonator photonpair sources on a silicon chip, Nature communications, 6 (2015).
[17] P. SENELLART, G. SOLOMON, AND A. WHITE, High-performance semiconductor quantum-dot single-photon sources, Nature nanotechnology, 12 (2017), p. 1026.
[18] Meyer-Scott E, Montaut N, Tiedau J, Sansoni L, Herrmann H, Bartley TJ, Silberhorn C. Limits on the heralding efficiencies and spectral purities of spectrally filtered single photons from photon-pair sources. *Phys Rev A*. 2017;**95**: Article 061803.
[19] J. WANG, S. PAESANI, Y. DING, R. SANTAGATI, P. SKRZYPCZYK, A. SALAVRAKOS, J. TURA, R. AUGUSIAK, L. MANCINSKA ˇ , D. BACCO, D. BONNEAU, J. W. SILVERSTONE, Q. GONG, A. ACÍN, K. ROTTWITT, L. K. OXENLØWE, J. L. O'BRIEN, A. LAING, AND M. G. THOMPSON, Multidimensional quantum entanglement with large-scale integrated optics, Science, 360 (2018), pp. 285–291.
[20] C. VIGLIAR, S. PAESANI, Y. DING, J. C. ADCOCK, J. WANG, S. MORLEY-SHORT, D. BACCO, L. K. OXENLØWE, M. G. THOMPSON, J. G. RARITY, AND A. & LAING, Logical qubits in a silicon photonic chip, Nature Physics , 17, pp. 1137–1143 (2021).